Analele Universităţii de Vest din Timişoara
Vol. L, 2007
Seria Fizică

OXIDE AND SILICATE NANOPHOSPHORS: SOFT CHEMICAL SYNTHESIS ROUTES AND LUMINESCENCE PROPERTIES

Miroslav D. Dramićanin

Vinča Institute of Nuclear Sciences, PO Box 522, 11001 Belgrade, Serbia

Abstract
Besides well-known quantum dots, lanthanide- and 3d metal-doped oxide and silicate nanocrystals form a new promising class of nanophosphors. Research is boosted by opto-electronic applications, such as lasers, displays and optical storage media, and medical diagnostic applications, such as scintillators and biological essays. This entry summarizes several soft chemical approaches for the synthesis of oxide and silicate nanophosphors with special emphases on salted sol-gel and combustion techniques. Structure and morphology of phosphor nanoparticles are highlighted as a basis for discussion of luminescence properties. Luminescence emission and lifetime data for several nanophosphors are presented. It is found that the luminescence properties of nanoparticles differ from corresponding bulk materials in several ways: (i) spectroscopic changes, as a systematic broadening of the luminescence bands, resulting from a structural disorder intrinsic to the small size, and (ii) an alternated luminescence lifetimes, due to due to the change in the refractive index and modification of energy transfers and cross relaxation processes.
Keywords: phosphors, nanomaterials, lanthanides, luminescence

1. Introduction

Luminescent materials, i.e. phosphors, emit radiation when stimulated with fast electrons, X-rays, ultraviolet (UV) photons, or some other form of radiation. Among them oxide and silicate hosts doped with rare earth (RE) and transition metal (TM) ions have important value due to low absorption of the host, easy processing into various forms and photostable emission. Within the last two decades these luminescent systems have been intensively studied with particular interest towards applications in optics, telecommunication and lighting. More recently, the developments of high resolution flat displays, and strong potential of inorganic phosphors to replace organic dyes, traditionally used as fluorescent markers in medicine, have increased the demand for the well structured, nanosized phosphor materials. At present there is a variety of well developed nanophosphors as well as numerous methods for their synthesis and processing [1]. In particular soft chemical methods, such as sol gel, precipitation, co-precipitation, spray and flame pyrolysis and combustion, are well recognized synthesis routes for inorganic phosphors. However, still a great concern has been

the successful nano-fabrication of phosphors, able to preserve high luminescence efficiency and thermo dynamical stability characteristic of their bulk counterparts, and to enhance their compatibility with advanced technology requirements.

Traditional phosphors are usually in powder form and are polycrystalline. The size of the particles are normally in tens (fine powder) to hundreds of micrometers. An “ultra fine powder” which is usually achieved by milling, is said to be less then 10 mm. Nanophosphor is a type of phosphor that has a dimension in between 1 and 100 nm. Nanostructured materials have turned into a class of their own in recent times with their properties being quite different from those of the corresponding bulk crystalline materials. During the past decade, optical properties of nanosized materials have attracted considerable interest. Stronger luminescence emission in nanocrystalline materials compared to bulk materials and modification of radiative lifetime have been reported [2]. It is shown that doping uniformity and phase purity are easier to achieve with nanomaterials [3]. Internal scattering in materials is reduced when the size of the phosphor particles is much smaller than the wavelength of the visible light. Nanophosphors can increase doping concentrations without quenching effect due to reduced energy transfer between identical or inequivalent emission centers [3].

2. Soft chemical methods for nanophosphors synthesis

One of common ways today to produce nanophosphors is to exploit some of soft chemical synthesis routes. The most common are: sol-gel, combustion, precipitation, co-precipitation, microemulsion, flame pyrolysis and aerosol synthesis. They offer many advantages over classical ceramic routes: in particular they utilize lower processing temperatures, fewer processing steps, reduced processing cost of materials, and many others. Here, a brief introduction to the first two of them is given.

2.1 Sol-gel

A process that has, in the past years, gained much notoriety in the glass and ceramic fields is the sol-gel reaction [4]. This chemistry produces a variety of inorganic networks from silicon or metal alkoxide monomer precursors. Sol-gel processing offers many advantages, including low processing temperature and molecular level homogeneity. The sol-gel reaction, as the name implies, involves the evolution of inorganic networks through the formation of a colloidal suspension (sol) and gelation of the sol to form a network in a continuous liquid phase (gel). The precursors for synthesizing these colloids consist of a metal or metalloid element surrounded by various reactive ligands. Metal alkoxides are most popular because

they react readily with water. The most widely used metal alkoxides are the alkoxysilanes, such as tetramethoxysilane (TMOS) and tetraethoxysilane (TEOS). However, other alkoxides such as aluminates, titanates, and borates are also commonly used in the sol-gel process, often mixed with TEOS, see Table 1.

Table 1. List of some commonly used metal alkoxides for sol-gel technology [1]

Name	Chemical formula
Tetraethoxysilane	$Si(OC_2H_5)_4$
Tetramethoxysilane	$Si(OCH_3)_4$
Titatanium (IV) isopropoxide	$Ti(OC_3H_7^{i})_4$
Titatanium (IV) etoxide	$Ti(OC_2H_5)_4$
Zinc isopropoxide	$Ti(OC_3H_7^{i})_2$
Aluminium *sec*-butoxide	$Al(OC_4H_9^{s})_3$
Aluminium isopropoxide	$Ti(OC_3H_7^{i})_3$
Triethyl borate	$B(OC_2H_5)_3$
Geraminum isopropoxide	$Ge(OC_3H_7^{i})_4$
Triethyl phosphate	$P(OC_2H_5)_3$
Gallium isporopoxide	$Ga(OC_3H_7^{i})_3$
Yttrium isporopoxide	$Y(OC_3H_7^{i})_3$
Zirconium *n*-butoxide	$Zr(OC_4H_9^{n})_3$
Rare-earth isopropoxide	$R(OC_3H_7^{i})_3$

Applying the sol-gel process, it is possible to fabricate ceramic or glass materials in a wide variety of forms: ultra-fine or spherical shaped powders, thin film coatings, ceramic fibers, microporous inorganic membranes, monolithic ceramics and glasses, or extremely porous aerogel materials. Thin films can be produced on a piece of substrate by spin-coating or dip-coating. When the "sol" is cast into a mold, a wet "gel" will form. With further drying and heat-treatment, the "gel" is converted into dense ceramic or glass articles. If the liquid in a wet "gel" is removed under a supercritical condition, a highly porous and extremely low density material called "aerogel" is obtained. As the viscosity of a "sol" is adjusted into a proper viscosity range, ceramic fibers can be drawn from the "sol". Ultra-fine and uniform ceramic powders are formed by precipitation, spray pyrolysis, or emulsion techniques. Regarding nanophoshor synthesis, additional advantage of sol-gel process is in that it allows for the fine control on the product's chemical composition, as even small quantities of

dopants, such as rare earth and 3d metals, can be introduced in the sol and end up in the final product finely dispersed.

2.2. Combustion

Combustion process is an exothermic reaction, which occurs with evaluation of light and heat [5, 6]. For any combustion, fuel and oxidizer are required. When the mixture of fuel and oxidizer are ignited, combustion takes place. Combustion is simply expressed by a well-known reaction, burning of carbon in presence of oxygen:

$$C + O_2 \rightarrow CO_2 + \text{heat}$$

Here carbon is reducer and oxygen is oxidizer. For nanophophor synthesis stoichiometric compositions of metal nitrates and fuels are calculated based upon propellant chemistry, see Table 2. For the reaction, an organic fuel is utilized, typically urea (CH_4N_2O), carbohydrazide (CH_6N_4O), or glycine ($C_2H_5NO_2$). Recently, polyethylene glycol (PEG) is successfully introduced. Along with classical function to facilitate combustion reaction PEG enables formation of size homogenous spherical particles by influencing a nucleation process of crystal. The nuclei, formed in a super-saturated solution with PEG, are strongly absorbed and surrounded by PEG chains. And nearly spherical shape of particle is therefore formed because of equal strain force from these chains in all directions around the nuclei. In addition, the adsorption of PEG polymer on the particle surfaces can prevent particle–particle aggregation due to steric hindrance effect.

Table 2. Oxidizing and reducing valencies of some metal nitrates and fuels [7].

Compound	Oxidizing/reducing valency
$M(NO_3)_2$	10-
$M(NO_3)_3$	15-
$M(NO_3)_4$	20-
NH_4NO_3	2-
Urea, CH_4N_2O	6+
Carbohydrazide, CH_6N_4O	8+
Oxalyl dihydrazide, $C_2H_6N_4O_2$	10+
3-Methyl Pyrazole 5-One, $C_4H_6N_2O$	20+
Dyformyl hydrazine, $C_2H_4N_2O_2$	8+
$Y(N_2H_3COO)_3$	12+
NH_4VO_3	3+

Saving energy is just one of many advantages that combustion synthesis holds over conventional techniques of materials production. The energy-consuming nature and size of furnaces limit the volume of material that can be converted. Combustion synthesis can yield objects of virtually any size, because the heat from the chemical reaction originates at every point inside the original sample. These reactions also attain temperatures anywhere from 1500 to 4000 ˚C, and the material heats at astounding rates of up to one million any combustion process reducer and oxidizer are required ˚C per second. That means combustion synthesis takes just a few seconds to turn a mixture of reactants into a new solid, as opposed to the minutes or even hours that furnaces, which rarely reach 2000 ˚C, require to do the same job. Intense and quick heating creates compounds with extremely uniform microscopic structures. In contrast, conventional furnaces heat material unevenly and can introduce flaws in the material's structure – a potentially fatal problem for an object that will experience tremendous stress.

3. Properties of some oxide and silicate nanophosphors

In this section properties of some oxide and silicate nanophorphors synthesized using soft chemical methods are presented with emphasize on the relation between their structural and luminescent properties.

3.1 $(Y,Gd)_2O_3:Eu^{3+}$ nanophosphor

Phosphors based on Eu^{3+} doped rare-earth (RE) sesquioxides such as yttrium, lanthanum and gadolinium are important materials with numerous applications in different fields. In particular, Eu^{3+} doped $(Y_x,Gd_{1-x})_2O_3$ is well-known luminescent material widely used to provide red light emission for modern optoelectronic devices [1, 8–11]. This material is synthesized using combustion method with PEG employed as fuel to achieve various compositions of solid state solutions (x = 0, 0.25, 0.5, 0.75 and 1); the details of synthesis are given in Ref. 12.

Morphology and particle sizes of all synthesized materials are checked with TEM. We found $(Y_x,Gd_{1-x})_2O_3:Eu^{3+}$ nanopowders in the form of particle agglomerates with dimensions of individual particles of about 40 nm, as show in Figure 1 for the case of $(Y_{0.75}Gd_{0.25})_2O_3$ sample.

XRD analysis confirms that all powders crystallize in cubic bixbyte type of structure - space group Ia3 (No. 206), Figure 2. In this structural type cations occupy two different crystallographic positions 8b (¼, ¼, ¼) with point symmetry $\bar{3}$ (S6, C_{3i}) and 24d (*x*, 0, ¼)

with point symmetry 2 (C_2). Both cations are octahedral coordinated. The oxygen ion, in the general 48e position, is tetrahedrally surrounded. Elementary cell is body centered with 16 formulae units.

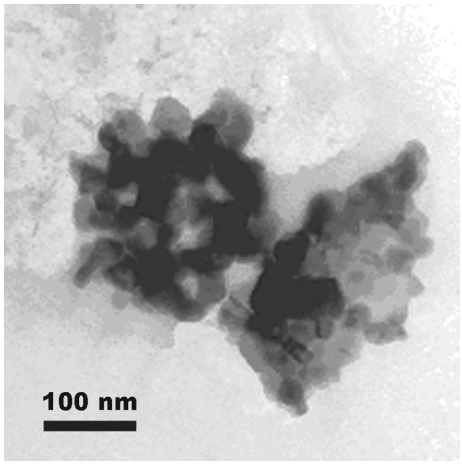

Fig 1. TEM image of $(Y_{0.75}Gd_{0.25})_2O_3:Eu^{3+}$ nanopowder sample.

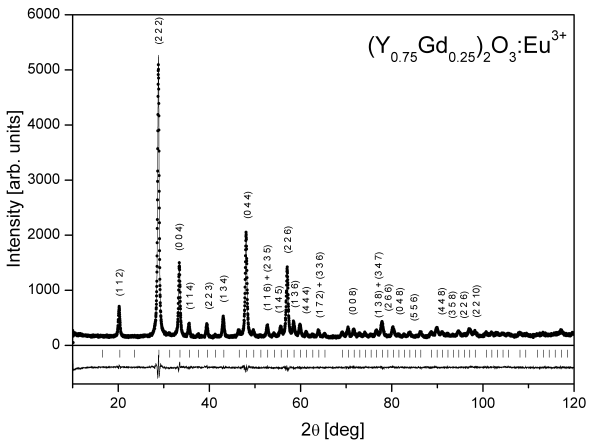

Fig 2. XRD pattern and Rietveld fit of the $(Y_{0.50}Gd_{0.50})_2O_3:Eu^{3+}$ nanopowder sample.

Luminescence emission spectra of all $(Y_x,Gd_{1-x})_2O_3:Eu^{3+}$ nanopowder samples (x = 1, 0.75, 0.5, 0.25 and 0) are presented on Figure 3. Measurements are performed with 1 ms time delay after the laser pulse in order to eliminate the contribution of the $^5D_1$ emission. Five characteristic bands centered at around 17223, 16853, 16345, 15860 and 14250 cm^{-1} associated to $^5D_0 \rightarrow {}^7F_i$ (i = 0, 1, 2, 3 and 4) spin forbidden f-f transitions, respectively, can be observed. In contrast to the S_6 site, there is no centre of inversion symmetry in the C_2 site. Then, the presence of inversion symmetry in the Eu^{3+} site drastically affects the luminescence spectra since in this case, induced electric dipole transitions cannot gain intensity by the mixing of opposite parity electron configuration with the $4f^N$ one. Therefore only few lines are due to Eu^{3+} in the S_6 sites and practically all the observed transition are due to the Eu^{3+} in C_2 sites. Measured spectra presented in Figure 3 have similar shape with small variations coming from difference in emission intensities and positions of $^5D_0 \rightarrow {}^7F_{0,1}$ transitions.

A focus on the emission spectra taken from 16600 cm^{-1} to 17400 cm^{-1} is given in Figure 4 in order to closely examine $^5D_0 \rightarrow {}^7F_1$ and $^5D_0 \rightarrow {}^7F_0$ transitions. One can observe a peak originating from $^5D_0 \rightarrow {}^7F_0$ transition of Eu^{3+} located in C_2 site at around 17223 cm^{-1} and from $^5D_0 \rightarrow {}^7F_1$ transition of Eu^{3+} located in S_6 site at around 17170 cm^{-1}. The later changes its value with change of mixed oxide composition from 17167 cm^{-1} for pure Y_2O_3 to 17182.4 cm^{-1} for Gd_2O_3. C_2 and S_6 sites differ from each other in the position of rare earth ion relative

to oxygen vacancy and the presence of inversion symmetry for S_6 site caused vanishing of the S_6 site luminescence. The electric dipole transitions can occur only by weak vibronic coupling. The relatively weak magnetic dipole transitions remain possible, but the selection rules restrict the possible transitions of this type through the $\Delta J = 0, \pm 1$ (except for $0 \leftrightarrow 0$) rule. Therefore for Eu^{3+} doped cubic sesquioxides only one line with very low intensity originates from Eu^{3+} ions in S_6 sites, and practically all observed transitions comes from Eu^{3+} ions in the C_2 sites. As expected from the knowledge of ion radius of Y^{3+} and Gd, the strongest splitting is observed for Y_2O_3.

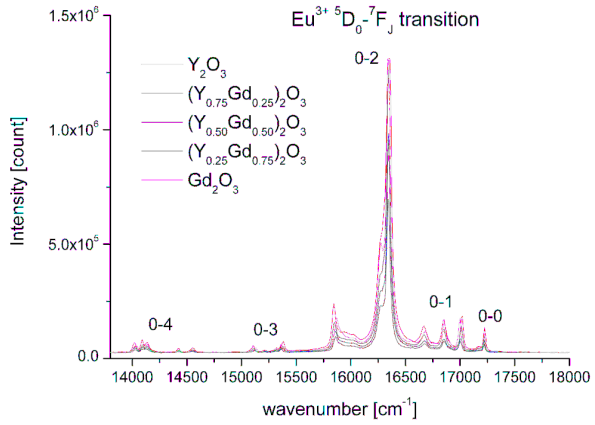

Fig 3. Luminescence emission spectra of $(Y,Gd)_2O_3:Eu^{3+}$ nanopowder.

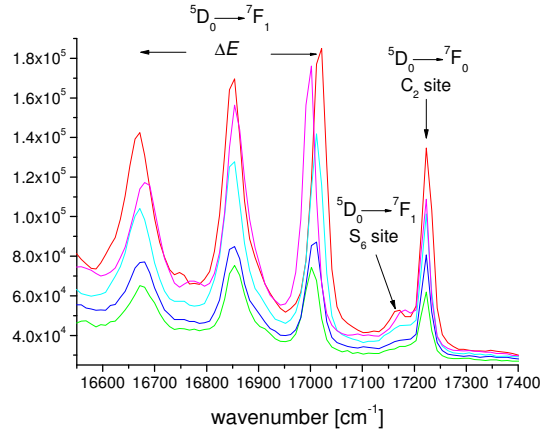

Fig 4. Stark components of the $^7F_1$ manifold of the Eu^{3+} emission.

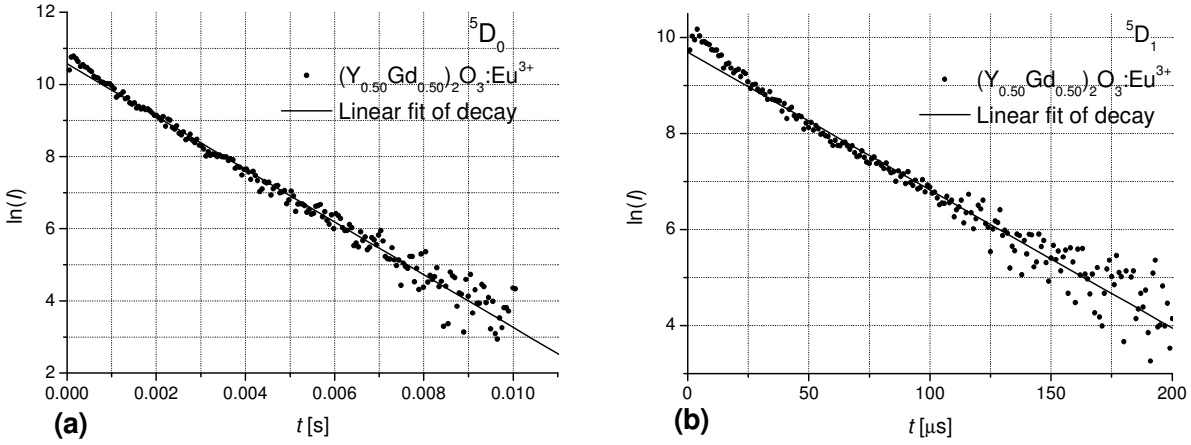

Fig. 5. Fluorescence decay profile for a) $^5D_0$ and b) $^5D_1$ level of $(Y_{0.5}Gd_{0.5})_2O_3:Eu^{3+}$ nanopowder.

Figure 5a shows the fluorescence decay curves of the $^5D_0$ emitting level obtained for the compound $(Y_{0.5}Gd_{0.5})_2O_3$ under excitation at 590 nm (λ_{em} = 612 nm). For investigated samples, fluorescence decay profiles could be adjusted by a single-exponential function and the obtained lifetimes are given in the Table 3.The lifetimes are 1.2 ms and 1.3 ms for pure Y_2O_3 and Gd_2O_3, and 1.5 for mixed oxides. These values are higher than the values obtained in the bulk (respectively 1 and 1.1 ms). There is several reasons to observe such difference and among them, a size effect, a refractive index variation in effective medium and a relative occupancy of the two sites. Shorter lifetimes are expected with the occupancy of the lower symmetry site (C_2 site), and this is observed on Figure 4 for the mixed $(Y_{0.25}Gd_{0.75})_2O_3$, $(Y_{0.50}Gd_{0.50})_2O_3$ and $(Y_{0.75}Gd_{0.25})_2O_3$ compounds. Concerning the $^5D_1$ lifetime (see Figure 5b), a quite high value of about 35 μs is obtained in the present work for all samples. In this case, cross relaxation effects, which is the major process involved in the reduction of the trivalent europium $^5D_1$ lifetimes, seems to be weak. This indicates homogeneous distribution of Eu^{3+} ions in nanoparticles.

3.2 Y_2SiO_5:Eu^{3+} nanophosphor

Yttrium oxyorthosilicate Y_2SiO_5 (YSO) is an important material exhibiting many valuable properties. Rare earth oxyorthosilicates (R_2SiO_5) doped with Eu^{3+}, Ce^{3+}, Pr^{3+}, Tb^{3+} and Yb^{3+} are well-known luminescent materials because of their cathodoluminescence, storage phosphor, scintillator and laser properties [13, 14]. In particular, Yb:Y_2SiO_5 have demonstrated efficient laser action and optical conversion exceeding 50% have been obtained [15]. It is also a promising candidate for coherent time-domain optical memory applications. This material is prepared by conventional sol-gel method, the details of synthesis are given in Ref. 16.

Rare earth oxyorthosilicates form two polymorphs, both of which are monoclinic. From La to Gd, they have the $P2_1/c$ space group, called the X_1 phases, and from Dy to Lu, they are found in the C2/c space group, and are called the X_2 phases. Tb and Y reportedly form both the X_1 and X_2 phases. The X_1 phase is a low-temperature phase, whereas the X_2 phase is the high-temperature one. In this structural type, all the ions occupy general 4e crystallographic sites with the local symmetry C_1. The Y^{3+} ions are in two non-equivalent site positions, one with coordination number (6+1) and mean Y-O distance of 2.309 Å and second with coordination number 6 and mean Y-O distance of 2.269 Å.

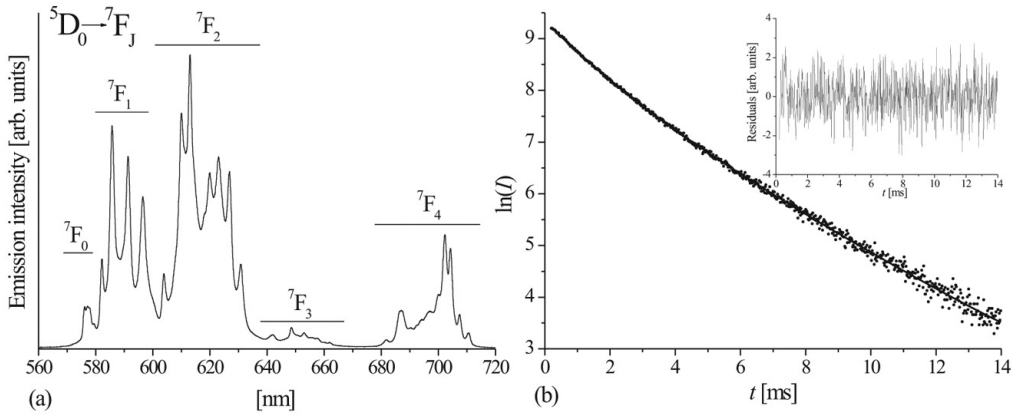

Fig. 6 a) Luminescence emission spectra of YSO:Eu^{3+} sample excited at 393 nm ($^5L_6$ level); b) $^5D_0$ emission decay. Residual for 2-exponentional fitting function is shown as inset (the decay times are found to be 1.5 and 2.9 ms).

As expected, two site occupancy corresponding to two different coordination of the Eu^{3+} ions is observed from the $^5D_0 \rightarrow {}^7F_0$ transition, Figure 6a. As Eu^{3+} and Y^{3+} have similar ionic radii, the site occupancy should be very close and the bands observed at about 577 and 578 nm are in agreement with the value reported in the literature for those two sites [17]. The lifetime measurements, Fig. 6b, exhibit double exponential behavior and justify assumption of two site occupancy.

3.3 $Zn_2SiO_4:Mn^{2+}$

The manganese-doped zinc orthosilicate, $Zn_2SiO_4:Mn^{2+}$, is an important material extensively used as a green luminescent phosphor in cathode ray tubes, lamps, and plasma display panels because of its high saturated color, very strong luminescence, long life span, lack of moisture sensitivity, and chemical stability. It can be used for medical imaging detectors for low-voltage radiography and fluoroscopy [18-20]. Manganese doped willemite nanophosphor is prepared using combination of sol-gel and combustion methods with details given in Ref. 21.

Zn_2SiO_4 under ordinary conditions crystallizes in phenacite structural type and belongs to the rhombohedral space group $R\bar{3}$, where all ions occupy general crystallographic positions [*x*, *y*, *z*] (18f in hexagonal axis set or 6f in rhombohedral axis set) with local symmetry 1. Since all the ions are in crystallographic positions of the same type to comply with stechiometry zinc ions will occupy two, silicon ions one and oxygen ions four different

18f (6f) crystallographic positions. In both non-equivalent crystallographic positions zinc ions are tetrahedrally coordinated with oxygen ions. This is important for understanding luminescence of $Zn_2SiO_4:Mn^{2+}$ because manganese ions substitute zinc in this structure. These two tetrahedrons are almost regular and very similar. They are graphically presented on Figure 7. Silicon ions are also tetrahedrally coordinated with oxygen ions in somewhat smaller and less regular tetrahedrons. Oxygen ions have less regular surroundings due to their strong deviation from close packaging, but essentially they have cationic triangular coordination with one silicon ion and two zinc ions.

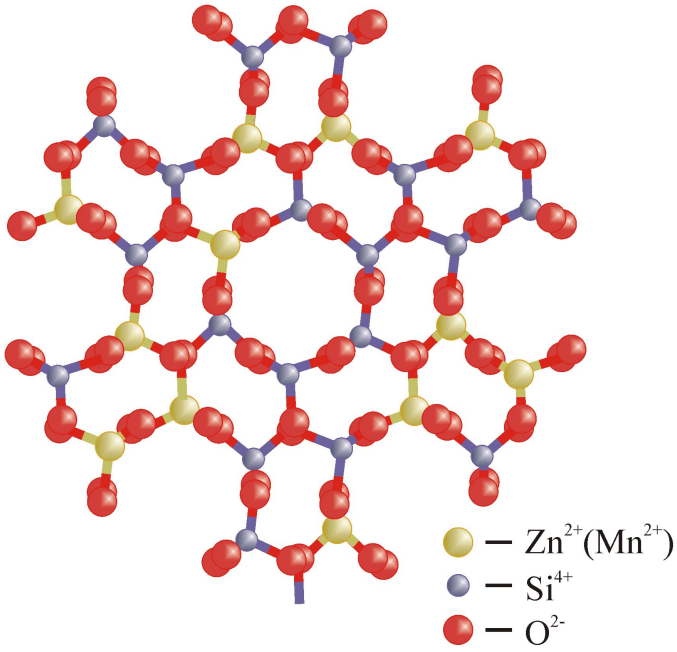

Fig. 7 The structure of Zn_2SiO_4.

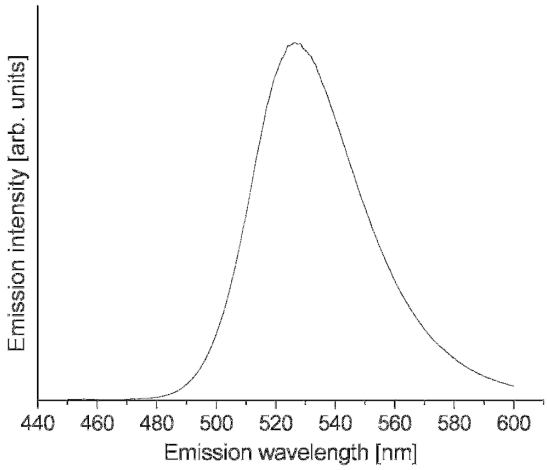

Fig. 8 Luminescence emission spectra of $Zn_2SiO_4:Mn^{2+}$ powder.

Luminescence due to Mn^{2+} is known to occur in more than 500 compounds. The Mn^{2+} has five electrons occupying the outermost 3d electron orbitals of the ion ($3d^5$ configuration). In tetrahedral coordination (weak crystal field) Mn^{2+} exhibits green luminescence from $^4T_1(G) \rightarrow {}^6A_1(S)$ transition. The position of the luminescence band maximum is influenced by the coordination change (covalency, interatomic distances, etc.) and by the concentration of Mn^{2+} in the host. Luminescence emission spectra of synthesized $Zn_2SiO_4:Mn^{2+}$ powder is presented on Fig. 8. The spectra shows characteristic emission with maximum situated at 526 nm. It should be noted that the emission spectrum does not have a simple gaussian shape due to some coordinate displacement of the potential energy curves. Fig. 8 shows a tailing in the long wavelength side of the emission band, in accordance with previous observation.

4. References

1. W.M. Yen, S. Shionoya and H. Yamamoto, "Phosphor Handbook," 2nd Edition, CRC Press, Boca Raton, (2007).
2. R.S. Meltzer, S.P. Feofilov, R. Tissue, H.B. Yuan, Phys. Rev. B. 60 (1999) 14012.
3. D. Jia, J.E. Weyant, C.V. Shaffer, A. Goonewardene, Y. Wang, X. Guo, K. Li, K. Zou and W. Jia, Nanotechnology. 1 (2006) 339.
4. C.J. Brinker and G.W. Scherer, "Sol-Gel Science: the Physics and Chemistry of Sol-Gel Processing," Academic Press, Sand Diego, 1990.
5. K.C. Patil, S.T. Aruna and S. Ekambaram, Curr. Opin. Solid State Mater. Sci. 2 (1997) 158.
6. Kashinath C. Patil, S.T. Aruna and T. Mimani, Curr. Opin. Solid State Mater. Sci. 6 (2002) 507.
7. S. Ekambaram, K.C. Patil, M. Maaza, „Synthesis of lamp phosphors: facile combustion approach", Journal of Alloys and Compounds 393 (2005) 8.
8. B. Bihari, H. Eilers and B. Tissue, J. Lumin. 75 (1997) 1.
9. R. Schmechel, M. Kennedy, H. von Seggem, H. Winkler, M. Kolbe, R. Fisher, L. Xaomao, A. Benker, M. Winterer and H. Hahn, J. Appl. Phys. 89 (2001) 1679.
10. P. Majewski, M. Rozumek, H. Schluckwerder and F. Aldinger, Int. J. Inorganic Mater. 3 (2001) 1343.
11. Garcia-Murillo, C. Luyer, C. Garapon, C. Dujardin, E. Bernstein, C. Pedrini and J. Mugnier, Opt. Mater. 19 (2002) 161.
12. Ž. Andrić, M.D. Dramićanin, M. Mitrić, V. Jokanović, A. Bessière and B. Viana, Opt. Mater. 30 (2008) 102.

13. C.Li, C.Wyon, R. Moncorge, IEEE J. Quant. Electron. 28 (1992) 1209.
14. T.E. Peters, J. Electrochem. Soc. 116 (1969) 985.
15. M. Jacquemet, C. Jacquemet, N. Janel, F. Druon, F. Balembois, P. Georges, J. Petit, B. Viana, D. Vivien, B. Ferrand, Appl. Phys. B 80 (2005) 171
16. R. Krsmanović, Ž. Andrić, M. Marinović-Cincović, I. Zeković and M.D. Dramićanin, Acta Phys. Polonica A, 112 (2007) 975.
17. C. Cannas, M. Mainas, A. Musinu, G. Piccaluga, A. Speghini and M. Bettinelli, Opt. Mat. 27 (2005) 1506.
18. Y. Kotera, J. Jpn. Soc. Color. Mater. 58 (1985) 80.
19. X. Ouyang, A.H. Kitai and T. Xiao, J. Appl. Phys. 79 (1996) 3229.
20. J. Lin, D.U. Sänger, M. Menning and K. Kärner, Mater. Sci. Eng. B 64 (1999) 73.
21. S.R. Lukić, D.M. Petrović, M.D. Dramićanin, M. Mitrić and Lj. Đačanin, Scripta Mater. 58 (2008) 655.